Taylor series expansion- and least square-based Lattice Boltzmann method: an efficient approach for simulation of incompressible viscous flows

C. Shu*, X.D. Niu, Y. Peng and Y.T. Chew
Department of Mechanical Engineering,
National University of Singapore, Singapore 119260
E-mail: mpeshuc@nus.edu.sg
*Corresponding author

Abstract: The Taylor series expansion- and least-square-based Lattice Boltzmann method (TLLBM) is a flexible Lattice Boltzmann approach capable of simulating incompressible viscous flows with arbitrary geometry. The method is based on the standard Lattice Boltzmann equation (LBE), Taylor series expansion and the least square optimisation. The final formulation is an algebraic form and essentially has no limitation on the mesh structure and lattice model. Successful applications of isothermal and thermal incompressible viscous flows have shown that the TLLBM is an efficient and promising version of LBM. In this paper, we will give the details of TLLBM and present some examples of its application.

Keywords: Lattice Boltzmann method; TLLBM; Taylor series expansion; least square approach; incompressible flow.

Reference to this paper should be made as follows: Shu, C., Niu, X.D., Peng, Y. and Chew, Y.T. (2005) 'Taylor series expansion- and least square-based Lattice Boltzmann method: an efficient approach for simulation of incompressible viscous flows', *Progress in Computational Fluid Dynamics*, Vol. 5, Nos. 1/2, pp.27–36.

Biographical notes: Dr. C. Shu is an Associate Professor in the Department of Mechanical Engineering, National University of Singapore. He obtained his BE and ME degrees in 1983 and 1986, respectively, from Nanjing University of Aeronautics and Astronautics (NUAA), P.R. China. After being a Lecturer in NUAA for two years, he went to University of Glasgow, UK, in October 1988 and obtained his PhD from the University of Glasgow in May 1991. From June 1991 to December 1991, he was a post-doctoral research fellow in the University of Glasgow. He joined NUS in January 1992. Dr. Shu has specialised in the computational fluid dynamics (CFD). Dr. Shu has published more than 80 papers in the SCI journals. His main interest includes development of efficient numerical methods to solve PDEs, and development and applications of Lattice Boltzmann method.

X.D. Niu is a Research Fellow in the Department of Mechanical Engineering, National University of Singapore. His main interest is in the development and application of Lattice Boltzmann method for micro-flows.

Y. Peng is a Research Fellow in the Department of Mechanical Engineering, National University of Singapore. Her main interest is in the development and application of Lattice Boltzmann method for thermal flows and turbulent flows.

Dr. Y.T. Chew is a Professor in the Department of Mechanical Engineering, National University of Singapore. He graduated from the University of Western Australia with BE (Hons) and ME in 1972 and 1973, respectively. He completed his PhD degree from Cambridge University in 1976 under the Cambridge's Pochobradsky Scholarship. He taught and conducted research on steady and unsteady separating boundary layer with

hot-wire and laser anemometers at University of Texas at Austin and Southern Methodist University, Dallas, USA, before joining NUS. He was Visiting Research Fellow at Virginia Polytechnic Institute and State University, and University College London in 1984–1985 and conducted research on hot-wire anemometry, boundary layer flows and bluff body aerodynamics. He is a consultant to several government bodies and firms in Singapore and Malaysia on wind effects on buildings and hydraulic modelling. His research interests are turbulence measurements; bluff body aerodynamics; wind effects on buildings and structures; bio-fluid dynamics; hot-wire and laser anemometry; particle image velocimetry.

1 INTRODUCTION

The development of the Lattice Boltzmann method (LBM) as an alternative computational fluid dynamics approach has attracted more and more attention in recent years [1]. However, because of the essential restriction of the standard Lattice Boltzmann equation (LBE) to the lattice-uniformity, the broad application of the LBM in engineering has been greatly hampered. For many practical problems, an irregular grid or a meshless structure is always preferable due to the fact that curved boundaries can be described more accurately, and that computational resources can be used more efficiently with it.

The drawback of the standard LBE restricting the lattice-uniformity comes from its precursor – the lattice gas cellular automata (LGCA) [2,3]. In the LGCA, the symmetry of lattice, which guarantees the isotropy of the fourth-order tensor consisting of particle velocities, is an essential condition to obtain the Navier-Stokes equations. By this condition, a particle at one lattice node must move to its neighbouring node in one time step. This is the condition of lattice-uniformity. Although the LBE [4,5] with Bhatnagar-Gross-Krook (BGK) [6] model has made great improvements over the LGCA, it also inherits the feature of lattice-uniformity, which makes it macroscopically similar to a uniform Cartesian-grid solver.

Theoretically, the feature of lattice-uniformity is not necessary to be kept because the distribution functions are continuous in physical space. In order to implement the LBE more efficiently for flows with arbitrary geometry, we proposed the Taylor series expansion- and least square-based Lattice Boltzmann method (TLLBM) [7,8]. TLLBM is actually based on the standard LBE [1], the well-known Taylor series expansion, the idea of developing Runge-Kutta method [9], and the least square optimisation [7]. The final form of our method is an algebraic formulation, in which the coefficients only depend on the coordinates of mesh points and lattice velocity, and are computed in advance. The new method is also free of lattice models. Theoretical analysis [10] for one-dimensional case showed that TLLBM could recover the Navier-Stokes equations with second order of accuracy.

In the past three years, the TLLBM has been successfully applied to simulate different isothermal and thermal incompressible viscous flows with arbitrary geometries [11–19]. The obtained numerical results are very accurate. It was found that the present method is an efficient and flexible approach for practical applications. In the following, we will describe the TLLBM and show some examples of its application.

2 TAYLOR SERIES EXPANSION- AND LEAST SQUARE-BASED LATTICE BOLTZMANN METHOD (TLLBM)

The TLLBM [7] is based on the well-known fact that the density distribution function is a continuous function in the physical space and can be well defined in any mesh system. Let us start with the standard LBE. The two-dimensional, standard LBE with BGK approximation can be written as

$$f_\alpha(x+e_{\alpha x}\delta t,\, y+e_{\alpha y}\delta t,\, t+\delta t) = f_\alpha(x,y,t)+\frac{f_\alpha^{\mathrm{eq}}(x,y,t)-f_\alpha(x,y,t)}{\tau},\quad \alpha=0,1,...,N, \tag{1}$$

where τ is the single relaxation time; f_α is the density distribution function along the α-direction; f_α^{eq} is its corresponding equilibrium state, which depends on the local macroscopic variables such as density ρ and velocity U(u, v); δt is the time step and $\mathrm{e}_\alpha(e_{\alpha x}, e_{\alpha y})$ is the particle velocity in the α-direction; N is the number of discrete particle velocities. Obviously, the standard LBE consists of two steps: collision and streaming. The macroscopic density ρ and momentum density ρU are defined as

$$\rho=\sum_{\alpha=0}^{N} f_\alpha\ ,\quad \rho\mathbf{U}=\sum_{\alpha=0}^{N} f_\alpha \mathbf{e}_\alpha \tag{2}$$

Suppose that a particle is initially at the grid point (x, y, t). Along the α-direction, this particle will stream to the position ($x + e_{\alpha x}\delta t$, $y + e_{\alpha y}\delta t$, t + δt). For a uniform lattice, $\delta x = e_{\alpha x}\delta_t$, $\delta y = e_{\alpha y}\delta_t$. So, ($x + e_{\alpha x}\delta_t$, $y + e_{\alpha y}\delta_t$) is at the grid point. In other words, equation (1) can be used to update the density distribution functions exactly at the grid points. However, for a non-uniform grid, ($x + e_{\alpha x}\delta_t$, $y + e_{\alpha y}\delta_t$) is usually not at the grid point ($x + \delta x$, $y + \delta y$). In the numerical simulation, we are only interested in the density distribution function at the mesh point for all the time levels. So, the macroscopic properties such as the density, flow velocity can be evaluated at every mesh point. To get the density distribution function at the grid point ($x + \delta x$, $y + \delta y$) and the time level $t + \delta t$, we need to apply the Taylor series expansion or other interpolation techniques. In this work, the Taylor series expansion is used. Note that the time level for the position ($x + e_{\alpha x}\delta_t$, $y + e_{\alpha y}\delta_t$) and the grid point ($x + \delta x$, $y + \delta y$) is the same, that is, $t + \delta t$. So, the expansion in the time direction is not necessary. As shown in Figure 1, for simplicity, we let point A represent the grid point (x_A, y_A, t), point A′ represent

the position ($x_A + e_{\alpha x}\delta t$, $y_A + e_{\alpha y}\delta t$, $t + \delta t$), and point P represent the position (x_p, y_p, $t + \delta t$) with $x_P = x_A + \delta x$, $y_P = y_A + \delta y$. So, equation (1) gives

$$f_\alpha(A', t+\delta t) = f_\alpha(A,t) + \left[f_\alpha^{\mathrm{eq}}(A,t) - f_\alpha(A,t) \right] / \tau \tag{3}$$

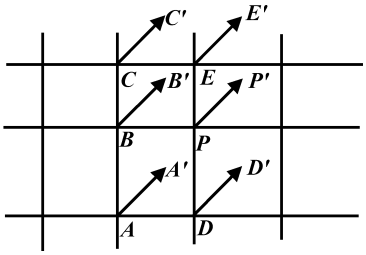

Figure 1 *Configuration of particle movement along the α-direction*

For the general case, A' may not coincide with the mesh point P. At first, we consider the Taylor series expansion with truncation to the first order derivative terms. So, $f_\alpha(A', t + \delta t)$ can be approximated by the corresponding function and its derivatives at the mesh point P as

$$f_\alpha(A', t+\delta t) = f_\alpha(P, t+\delta t) + \Delta x_A \frac{\partial f_\alpha(P, t+\delta t)}{\partial x} + \Delta y_A \frac{\partial f_\alpha(P, t+\delta t)}{\partial y} + O[(\Delta x_A)^2, (\Delta y_A)^2] \tag{4}$$

where $\Delta x_A = x_A + e_{\alpha x}\delta t - x_P$, $\Delta y_A = y_A + e_{\alpha y}\delta t - y_P$. Note that the above approximation has a truncation error of the second order. Substituting equation (4) into equation (3) gives

$$f_\alpha(P, t+\delta t) + \Delta x_A \frac{\partial f_\alpha(P, t+\delta t)}{\partial x} + \Delta y_A \frac{\partial f_\alpha(P, t+\delta t)}{\partial y} = f_\alpha(A,t) + \frac{f_\alpha^{\mathrm{eq}}(A,t) - f_\alpha(A,t)}{\tau} \tag{5}$$

It is indicated that equation (5) is a first order differential equation, which only involves two mesh points A and P. When a uniform grid is used, $\Delta x_A = \Delta y_A = 0$, equation (5) is reduced to the standard LBE (3). Solving equation (5) can provide the density distribution functions at all the mesh points. In this work, we try to develop an explicit formulation to update the distribution function. In fact, our new development is inspired from the Runge-Kutta method [9]. As we know, the Runge-Kutta method is developed to improve the Taylor series method in the solution of ordinary differential equations (ODEs). Like equation (5), Taylor series method involves evaluation of different orders of derivatives to update the functional value at the next time level. For a complicated expression of given ODEs, this application is very difficult. To improve the Taylor series method, the Runge-Kutta method evaluates the functional values at some intermediate points between time level t and the time level $t + \delta t$ and then combines them (through the Taylor series expansion) to form a scheme with the same order of accuracy. With this idea in mind, we look at equation (5). We know that at the time level $t + \delta t$, the density distribution function and its derivatives at the mesh point P are all unknowns. So, equation (5) has three unknowns in total. To solve for the three unknowns, we need three equations. However, equation (5) just provides one equation. We need two additional equations to close the system. As shown in Figure 1, we can see that along the α-direction, the particles at two mesh points P, B at the time level t will stream to the new positions P', B' at the time level $t + \delta t$. The distribution functions at these new positions can be computed through equation (1), which are given below

$$f_\alpha(P', t+\delta t) = f_\alpha(P,t) + \left[f_\alpha^{\mathrm{eq}}(P,t) - f_\alpha(P,t) \right] / \tau \tag{6}$$

$$f_\alpha(B', t+\delta t) = f_\alpha(B,t) + \left[f_\alpha^{\mathrm{eq}}(B,t) - f_\alpha(B,t) \right] / \tau \tag{7}$$

Using Taylor series expansion with truncation to the first order derivative terms, $f_\alpha(P', t + \delta t)$, $f_\alpha(B', t + \delta t)$ in above equations can be approximated by the function and its derivatives at the mesh point P. As a result, equations (6)–(7) can be reduced to

$$f_\alpha(P, t+\delta t) + \Delta x_P \frac{\partial f_\alpha(P, t+\delta t)}{\partial x} + \Delta y_P \frac{\partial f_\alpha(P, t+\delta t)}{\partial y} = f_\alpha(P,t) + \frac{f_\alpha^{\mathrm{eq}}(P,t) - f_\alpha(P,t)}{\tau} \tag{8}$$

$$f_\alpha(P, t+\delta t) + \Delta x_B \frac{\partial f_\alpha(P, t+\delta t)}{\partial x} + \Delta y_B \frac{\partial f_\alpha(P, t+\delta t)}{\partial y} = f_\alpha(B,t) + \frac{f_\alpha^{\mathrm{eq}}(B,t) - f_\alpha(B,t)}{\tau} \tag{9}$$

where $\Delta x_P = e_{\alpha x}\delta t$, $\Delta y_P = e_{\alpha y}\delta t$,

$$\Delta x_B = x_B + \mathrm{e}_{\alpha x}\delta t - x_P,\ \Delta y_B = y_B + \mathrm{e}_{\alpha y}\delta t - y_P$$

Equations (5), (8)–(9) form a system to solve for three unknowns. The solution of this system gives

$$f_\alpha(P, t+\delta t) = \Delta_P / \Delta \tag{10}$$

where

$$\Delta = \Delta x_A \Delta y_B - \Delta x_B \Delta y_A + \Delta x_B \Delta y_P - \Delta x_P \Delta y_B + \Delta x_P \Delta y_A - \Delta x_A \Delta y_P$$

$$\Delta_P = (\Delta x_A \Delta y_B - \Delta x_B \Delta y_A) g_P + (\Delta x_B \Delta y_P - \Delta x_P \Delta y_B) g_A + (\Delta x_P \Delta y_A - \Delta x_A \Delta y_P) g_B$$

$$g_P = f_\alpha(P,t) + \left[f_\alpha^{\mathrm{eq}}(P,t) - f_\alpha(P,t) \right] / \tau$$

$$g_A = f_\alpha(A,t) + \left[f_\alpha^{\mathrm{eq}}(A,t) - f_\alpha(A,t) \right] / \tau$$

$$g_B = f_\alpha(B,t) + \left[f_\alpha^{\mathrm{eq}}(B,t) - f_\alpha(B,t) \right] / \tau$$

Note that g_P, g_A, g_B are actually the post-collision state of the distribution function at the time level t and the mesh point P, A, B, respectively. Equation (10) has the second order of truncation error, which may introduce a large numerical diffusion. To improve the accuracy of numerical computation, we need to truncate the Taylor series expansion to include the second order derivative terms. For the two-dimensional case, this expansion involves six unknowns, that is, one distribution function, two first order derivatives, and three second order derivatives at the time level $t + \delta t$. To solve for these unknowns, we need six equations to close the system. This can be done by applying the second order Taylor series expansion at six points. As shown in Figure 1, the particles at six mesh points P, A, B, C, D, E at the time level t will stream to positions P', A', B', C', D', E' at the time level $t + \delta t$. The distribution functions at these new positions can be computed through equation (1). Then, by using the second order Taylor series expansion at these new positions in terms of the distribution function and its derivatives at the mesh point P, we can get the following equation system

$$g_i = \{s_i\}^T \{V\} = \sum_{j=1}^{6} s_{i,j} V_j, \quad i = P, A, B, C, D, E \tag{11}$$

where

$$g_i = f_\alpha(x_i, y_i, t) + \left[f_\alpha^{\mathrm{eq}}(x_i, y_i, t) - f_\alpha(x_i, y_i, t) \right] / \tau$$

$$\{s_i\}^T = \{1, \Delta x_i, \Delta y_i, (\Delta x_i)^2/2, (\Delta y_i)^2/2, \Delta x_i \Delta y_i\}$$

$$\{V\} = \{f_\alpha, \partial f_\alpha/\partial x, \partial f_\alpha/\partial y, \partial^2 f_\alpha/\partial x^2, \partial^2 f_\alpha/\partial^2 y, \partial^2 f_\alpha/\partial x \partial y\}^T$$

g_i is the post-collision state of the distribution function at the ith point and the time level t, $\{s_i\}^T$ is a vector with six elements formed by the coordinates of mesh points, $\{V\}$ is the vector of unknowns at the mesh point P and the time level $t + \delta t$, which also has six elements, s_{ij} is the jth element of the vector $\{s_i\}^T$ and V_j is the jth element of the vector $\{V\}$. Our target is to find its first element $V_1 = f_\alpha(P, t + \delta t)$. Equation system (11) can be put into the following matrix form

$$[\mathrm{S}]\{V\} = \{g\} \tag{12}$$

where

$$\{g\} = \{g_P, g_A, g_B, g_C, g_D, g_E\}^T$$

$$[S] = [s_{i,j}] = \begin{bmatrix} \{s_P\}^T \\ \{s_A\}^T \\ \{s_B\}^T \\ \{s_C\}^T \\ \{s_D\}^T \\ \{s_E\}^T \end{bmatrix} = \begin{bmatrix} 1 & \Delta x_P & \Delta y_P & (\Delta x_P)^2/2 & (\Delta y_P)^2/2 & \Delta x_P \Delta y_P \\ 1 & \Delta x_A & \Delta y_A & (\Delta x_A)^2/2 & (\Delta y_A)^2/2 & \Delta x_A \Delta y_A \\ 1 & \Delta x_B & \Delta y_B & (\Delta x_B)^2/2 & (\Delta y_B)^2/2 & \Delta x_B \Delta y_B \\ 1 & \Delta x_C & \Delta y_C & (\Delta x_C)^2/2 & (\Delta y_C)^2/2 & \Delta x_C \Delta y_C \\ 1 & \Delta x_D & \Delta y_D & (\Delta x_D)^2/2 & (\Delta y_D)^2/2 & \Delta x_D \Delta y_D \\ 1 & \Delta x_E & \Delta y_E & (\Delta x_E)^2/2 & (\Delta y_E)^2/2 & \Delta x_E \Delta y_E \end{bmatrix}$$

$$\Delta x_C = x_C + e_{\alpha x}\delta t - x_P, \Delta y_C = y_C + e_{\alpha y}\delta t - y_P$$

$$\Delta x_D = x_D + e_{\alpha x}\delta t - x_P, \Delta y_D = y_D + e_{\alpha y}\delta t - y_P$$

$$\Delta x_E = x_E + e_{\alpha x}\delta t - x_P, \Delta y_E = y_E + e_{\alpha y}\delta t - y_P$$

The expressions of Δx_P, Δy_P, Δx_A, Δy_A, Δx_B, Δy_B have been given previously. Since [S] is a 6×6 dimensional matrix, it is very difficult to get an analytical expression for the solution of equation system (12). We need to use a numerical algorithm to get the solution. Note that the matrix $[S]$ only depends on the coordinates of mesh points, which can be computed once and stored for the application of equation (12) at all time levels.

In practical applications, it was found that the matrix $[S]$ might be singular or ill-conditioned. To overcome this difficulty and make the method be more general, we introduce the least square approach [10] to optimise the approximation by equation (11). Equation (11) has six unknowns (elements of the vector $\{V\}$). If equation (11) is applied at more than six mesh points, then the system is over-determined. For this case, the unknown vector can be decided from the least square method. For simplicity, let the mesh point P be represented by the index $i = 0$, and its adjacent points be represented by index $i = 1,2, \ldots, M$, where M is the number of neighbouring points around P and larger than five. At each point, we can define an error in terms of equation (11), that is,

$$err_i = g_i - \sum_{j=1}^{6} s_{i,j} V_j, \quad i = 0,1,2, \ldots, M \tag{13}$$

The square sum of all the errors is defined as

$$E = \sum_{i=0}^{M} err_i^2 = \sum_{i=0}^{M} \left(g_i - \sum_{j=1}^{6} s_{i,j} V_j \right)^2 \tag{14}$$

To minimise the error E, we need to set $\partial E / \partial V_k = 0, k = 1,2,...,6$, which leads to

$$[S]^T [S]\{V\} = [S]^T \{g\} \tag{15}$$

where $[S]$ is a $(M+1) \times 6$ dimensional matrix, which is given as

$$[S] = \begin{bmatrix} 1 & \Delta x_0 & \Delta y_0 & (\Delta x_0)^2/2 & (\Delta y_0)^2/2 & \Delta x_0 \Delta y_0 \\ 1 & \Delta x_1 & \Delta y_1 & (\Delta x_1)^2/2 & (\Delta y_1)^2/2 & \Delta x_1 \Delta y_1 \\ - & - & - & - & - & - \\ - & - & - & - & - & - \\ - & - & - & - & - & - \\ 1 & \Delta x_M & \Delta y_M & (\Delta x_M)^2/2 & (\Delta y_M)^2/2 & \Delta x_M \Delta y_M \end{bmatrix}_{(M+1)\times 6}$$

and $\{g\} = \{g_0, g_1, \ldots, g_M\}^T$

The Δx and Δy values in the matrix $[S]$ are given as

$$\Delta x_0 = e_{\alpha x}\delta t,\ \Delta y_0 = e_{\alpha y}\delta t \tag{16a}$$

$$\Delta x_i = x_i + e_{\alpha x}\delta t - x_0,\ \Delta y_i = y_i + e_{\alpha y}\delta t - y_0,\quad \text{for } i = 1, 2, \ldots, M \tag{16b}$$

Clearly, when the coordinates of mesh points are given, and the particle velocity and time step size are specified, the matrix $[S]$ is determined. Then from equation (15), we obtain

$$\{V\} = ([S]^T[S])^{-1}[S]^T\{g\} = [A]\{g\} \tag{17}$$

Note that $[A]$ is a $6 \times (M+1)$ dimensional matrix. From equation (17), we can obtain

$$f_\alpha(x_0, y_0, t + \delta t) = V_1 = \sum_{k=1}^{M+1} a_{1,k}^{\alpha} g_{k-1}^{\alpha} \tag{18}$$

where $a_{1,k}^{\alpha}$ are the elements of the first row of the matrix $[A]$, which are pre-computed before the LBM is applied. Therefore, little computational effort is introduced as compared with the standard LBE. Note that the function g is evaluated at the time level t. So, equation (18) is actually an explicit form to update the distribution function at the time level $t + \delta t$ for any mesh point. In the above process, there is no requirement for the selection of neighbouring points. In other words, equation (18) has nothing to do with the mesh structure. It only needs to know the coordinates of the mesh points. Thus, we can say that equation (18) is basically a meshless form. It is obvious from equation (18) that no differential equation and its resultant algebraic equations are involved in the TLLBM. TLLBM only involves in the algebraic operation, which is considered as the major advantage of the standard LBM.

We have carried out a theoretical analysis for the error of TLLBM [7] through a one-dimensional case and found that TLLBM could recover Navier-Stokes equations with second order of accuracy.

3 APPLICATIONS OF TLLBM TO SIMULATE ISOTHERMAL INCOMPRESSIBLE FLOWS

Therefore, at each mesh point, for each particle direction, we need only in this part to show some applications of TLLBM for simulation of incompressible, isothermal flows with the use of non-uniform grids. Although the proposed method has meshless feature, a structured grid is recommended to be used. This is because in our method, only the coordinates of mesh points are involved. When a structured grid is used, it is much easier for us to define the coordinates of mesh points. In our application, we use a structured grid, and take M as 8 for convenience. As shown in Figure 2, for an internal mesh point (i, j) (noted as '0' in equation (18)), the eight neighbouring points are taken as $(i-1, j-1)$; $(i-1, j)$; $(i-1, j+1)$; $(i, j-1)$; $(i, j+1)$, $(i+1, j-1)$; $(i+1, j)$; $(i+1, j+1)$. Therefore, at each mesh point, we only need to store nine coefficients $a_{1,k}$, $k = 1,2, \ldots, 9$ before equation (18) is applied.

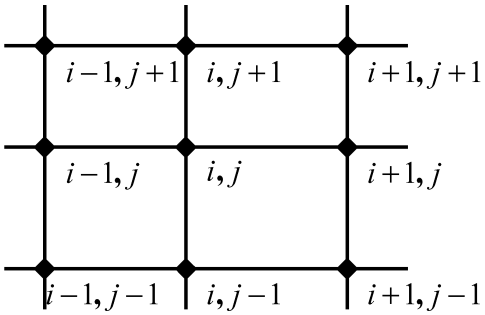

Figure 2 *Schematic plot of neighbouring point distribution around the point (i, j)*

3.1 2D square and polar cavity flows

For these two cases, the lid moves with a constant velocity of $U = 0.15$. The Reynolds number is defined as $\mathrm{Re} = UL/\upsilon$ (based on the lid velocity and the characteristic length of the cavity). Initially, a constant density, $\rho = 1$, is prescribed in the whole field, and the velocities in the interior of the cavity are set to zero. At the end of each time step, the density distribution function f_α on the moving wall is set to the equilibrium state. The whole halfway wall bounce back boundary conditions are used on the other three stationary walls. Figures 3 and 4 show the streamlines and velocity profiles along vertical and horizontal central lines of the square cavity at Re = 10000, respectively. Our LBM results compare well with those of Navier-Stokes solver [20]. Figure 5 shows the comparison of radial (u_r) and azimuthal (u_g) velocity profiles along the line of $\theta = 0°$ in the polar cavity at Re = 350. Again, the LBM results are in good agreement with the experimental and numerical data of Fuchs and Tillmark [21]. The detailed simulation results of these two cases can be found in [11].

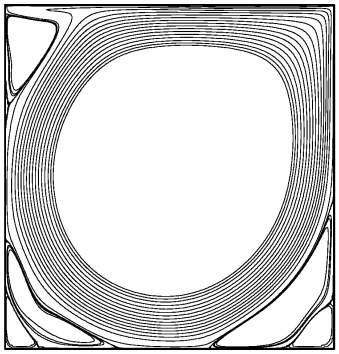

Figure 3 *Streamlines of lid-driven square cavity flow at Re = 10000 (mesh size: 145 × 145)*

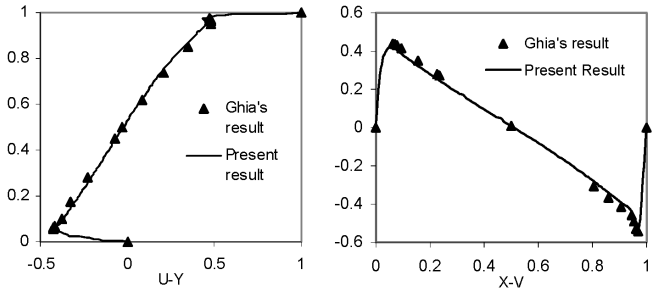

Re = 10000, 145×145

Figure 4 *U (left) and V (right) velocity profiles along vertical and horizontal central lines of the square cavity at Re = 10000 (mesh size: 145 × 145)*

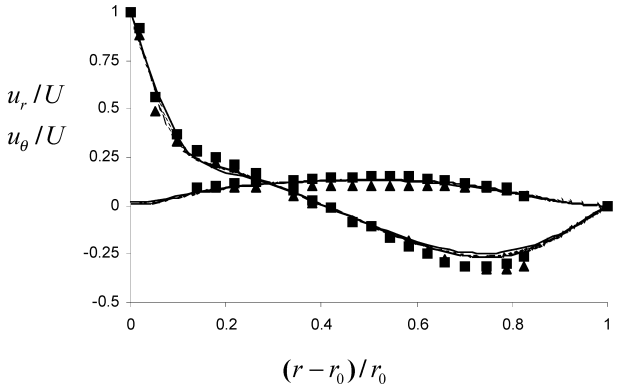

Figure 5 *Comparison of radial (u_r) and azimuthal (u_q) velocity profiles along the line of θ = 0° in the polar cavity at Re = 350 (■ numerical data by Fuchs and Tillmark; ▲ experimental data by Fuchs and Tillmark; —— Present result of 49 × 49; – – – Present result of 65 × 65; — – — Present result of 81 × 81)*

3.2 3D cubic cavity flows

The two-dimensional form of TLLBM has also been extended to the three-dimensional case, which is applied to simulate the driven flow in a cubic cavity. Figure 6 displays the velocity profiles of the *u* component on the vertical central line and the *v* component on the horizontal central line on the plane of *z* = 0.5 in a cubic cavity at Re = 400. All the results are compared well with those of Ku et al. [22]. To show the three-dimensional effect, the 2D results obtained by the TLLBM are also included in Figure 6.

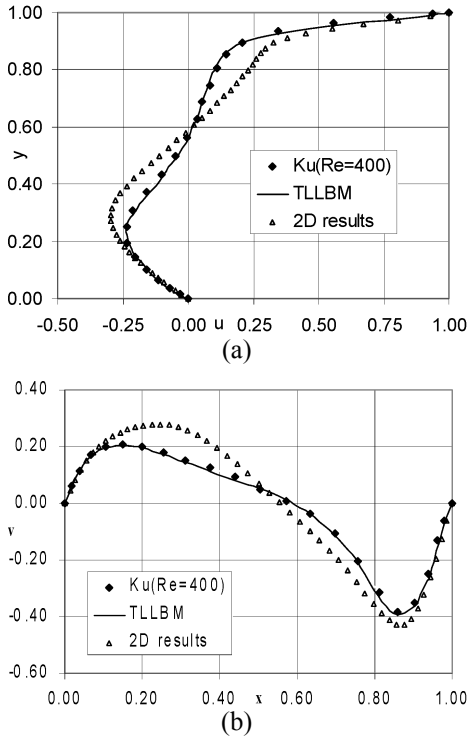

Figure 6 *3D cavity velocity profiles for Re = 400 (mesh size: 49 × 49 × 49) (a) u component on vertical central line; (b) v component on horizontal central line. The details of TLLBM work for this case can be referred to [13].*

3.3 Steady flow and early stage of flows around a circular cylinder

To show the capability of TLLBM for simulation of flows with curved boundary, we consider the steady flow past a circular cylinder at low Reynolds numbers. Figures 7, 8 and 9 show some results of flow around a circular cylinder at Re = 20 and 40. In our simulations, the far field boundary is set at 50.5 diameter away from the centre of the cylinder and a 241 × 181 O-type grid is used. With this grid distribution, the time step, in units of $D/(2U_\infty)$, is equal to 0.00375, and the maximum grid stretch ratio r_{max} (defined as the ratio of the maximum mesh spacing over the minimum mesh spacing) is 160.7. Clearly, our TLLBM results agree well with the experimental data of Coutanceu and Bouard [23].

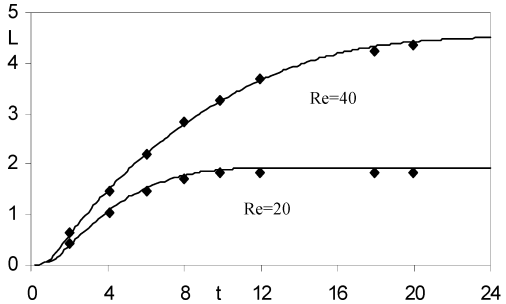

Figure 7 *Time evolution of the wake length for different Reynolds numbers (♦ Experimental data by Coutanceu and Bouard; —— TLLBM results)*

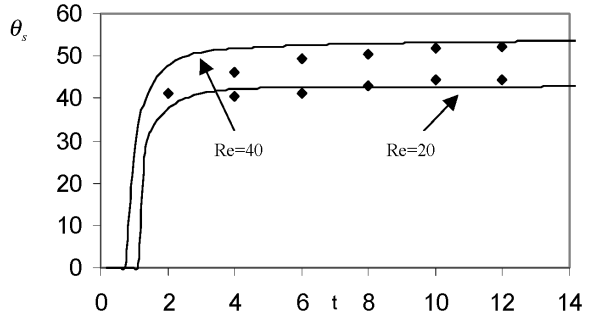

Figure 8 *Time evolution of the separation angle for different Reynolds numbers (♦ Experimental data by Coutanceu and Bouard; —— TLLBM results)*

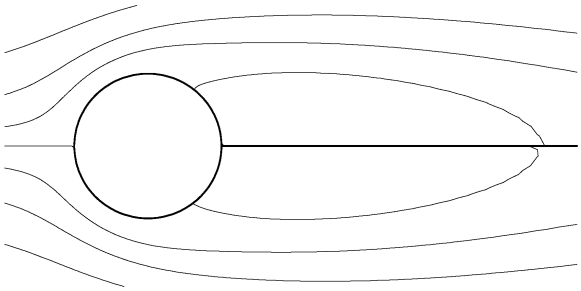

Figure 9 *Streamlines of the final steady state at Re = 40*

Figures 10, 11 and 12 show some results for flow around an impulsively started cylinder at Re = 550, 3000 and 9500. The flow around an impulsively started circular cylinder at these three Reynolds numbers is known to develop eventually the three-dimensional phenomenon. However, careful flow visualisation reveals that the flow in the early stage of development in the laminar wake region is still two-dimensional. In our simulations, for Reynolds numbers of 550 and 3000, the outer boundary is placed at 15.5 diameter away from the centre of the cylinder, the grid size is taken as 241 × 121 with the maximum grid stretch ratio of $r_{max} = 159$, and the time step, in units of $D/(2U_\infty)$, is equal to 0.001875. For the Reynolds number of 9500, the corresponding parameters are taken as 3, 241 × 301 with $r_{max} = 6.7$ and $\Delta t = 0.00075$, respectively. As can be seen from Figures 10–12, the TLLBM results are in good agreement with the experimental data of Bouard and Coutanceau [24], Loc and Bouard [25] and Chang and Chern [26]. The details of the above work can be found in [14].

Figure 10 *Instantaneous streamlines (left) and vorticity contours (right) of Re = 9500 at t = 4s (Dash line represents the negative vorticity)*

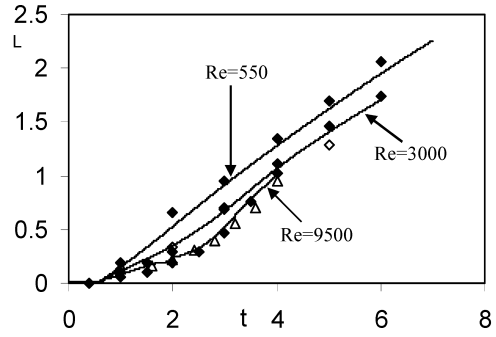

Figure 11 *Time evolution of the wake length for moderate and high Reynolds numbers (◆ Experimental data of Bouard and Coutanceau; ◇ and △ Results of Loc and Bouard for Re=3000 and 9500)*

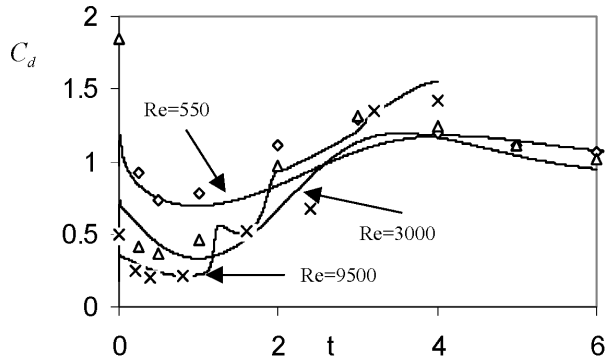

Figure 12 *Time evolution of the drag coefficient for different numbers (Symbols are the results of Chang and Chern for Re=550 (◇), 3000 (△), 9500 (×); —— TLLBM results)*

3.4 Unsteady flows in a square cavity and flows around a circular cylinder

The TLLBM has also been applied to simulate unsteady flows to test its time accuracy. We first consider the simulation of the oscillating flow in a square lid-driven cavity by using TLLBM. A periodic lid velocity with a sinusoidal waveform $u(t) = U\cos(\omega t)$ (U is the maximum lid velocity during the cycle, ω is the frequency of the oscillation and t is the time) is imposed on the lid. The period of oscillation, T, is related to the frequency by $T = 2\pi/\omega$.The simulation is performed with Re = 400, frequency of $\omega = 1$ and $U = 0.15$. A non-uniform grid of 97 × 97 with stretching near the boundaries is used, and as a consequence, the time step is set as, in the unit of L/U, 4.5×10^{-4}. The oscillatory flow reaches the periodic state when the velocity components u and v of each point in the domain at two consequent flow cycles are with a small tolerance of $\varepsilon = 10^{-5}$. The flow reaches periodic state after seven cycles. The instantaneous streamlines obtained by TLLBM at different times in a period are shown in Figure 13.

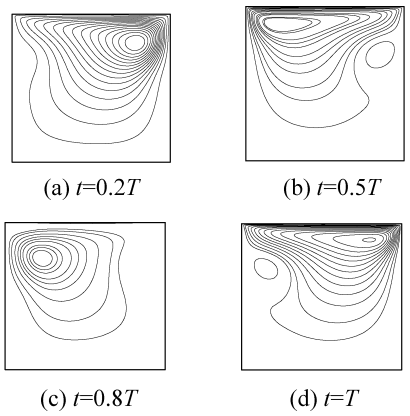

Figure 13 *Instantaneous streamlines at different times in a period for the present method*

Our study was also extended to the simulation of two-dimensional vortex shedding behind a circular cylinder. The grid of 241 × 241 is used. The far field is set at 25.5 diameter away from the centre of the cylinder and the time step, in units of $D/(2U)$, is equal to 0.00375. Figure 14 shows the sequence of vortex shedding over a complete cycle using a sequence of instantaneous streamlines and vorticity distributions at different times in a period of the shedding cycle. The details of the above work are shown in [11].

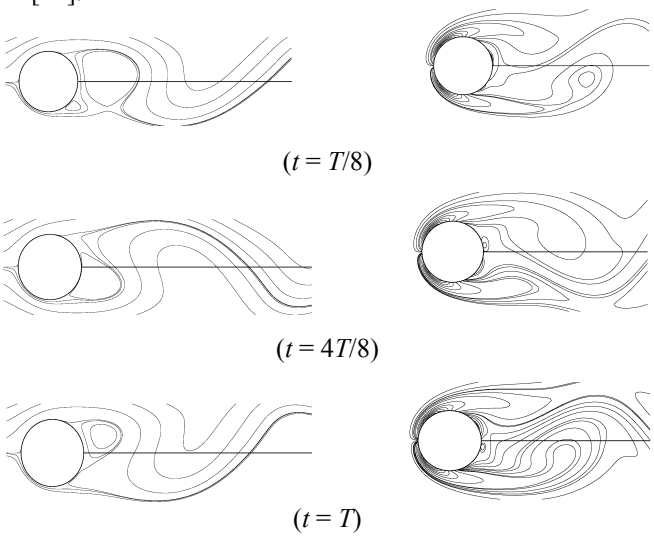

Figure 14 *Streamlines (left) and vorticity contours (right) near the wake at different times in a period for flows at Re = 100*

4 APPLICATIONS OF TLLBM TO SIMULATE THERMAL INCOMPRESSIBLE FLOWS

TLLBM has also been successfully applied in the incompressible thermal flows. The thermal model used is the internal energy density distribution function (IEDDF) model proposed by He et al. [27]. The governing equations for the two density distribution functions are

$$\overline{f}_\alpha(x+e_\alpha\delta t,t+\delta t)-\overline{f}_\alpha(x,t) = -\frac{\delta t}{\tau_v+0.5\delta t}\left[\overline{f}_\alpha(x,t)-f_\alpha^{\mathrm{eq}}(x,t)\right]+\frac{\tau_v F_\alpha\delta t}{\tau_v+0.5\delta t} \tag{19}$$

$$\overline{g}_\alpha(x+e_\alpha\delta t,t+\delta t)-\overline{g}_\alpha(x,t) = -\frac{\delta t}{\tau_c+0.5\delta t}\left[\overline{g}_\alpha(x,t)-g_\alpha^{\mathrm{eq}}(x,t)\right]-\frac{\tau_c f_\alpha q_\alpha\delta t}{\tau_c+0.5\delta t} \tag{20}$$

When equations (19) and (20) are used on an arbitrary mesh, $(x + e_{\alpha x}\delta t,\ y + e_{\alpha y}\delta t)$ is usually not at the grid point $(x + \delta x,\ y + \delta y)$. To solve this problem, the TLLBM technique can be applied to these two equations [17] following the same procedure as shown in Section 2, which results in

$$\overline{f_\alpha}(x_0,y_0,t+\delta t)=W_1=\sum_{k=1}^{M+1}a_{1,k}\,\overline{f_{k-1}}' \tag{21}$$

$$\overline{g_\alpha}(x_0,y_0,t+\delta t)=W_1'=\sum_{k=1}^{M+1}a_{1,k}'\,\overline{g_{k-1}}' \tag{22}$$

where

$$\{W'\}=\{\overline{g_\alpha},\partial\overline{g_\alpha}/\partial x,\partial\overline{g_\alpha}/\partial y,\partial^2\overline{g_\alpha}/\partial x^2,\ \partial^2\overline{g_\alpha}/\partial^2 y,\partial^2\overline{g_\alpha}/\partial x\partial y\}^T$$

When the same particle velocity model and the same neighbouring points are chosen for these two distribution functions, the geometric matrices A and A' are the same, which can save both the computational time and the storage space.

In the following, we will show some simulation results using the TLLBM. All the results are based on the non-uniform grids.

4.1 Natural convection in a two-dimensional square cavity

In a two-dimensional square cavity, the two sidewalls are maintained at different temperatures. The temperature difference between the walls introduces a temperature gradient in the fluid, and the consequent density difference induces a fluid motion, that is, convection. The top and bottom walls are adiabatic.

Figure 15 shows the streamlines and isotherms of $Ra = 10^6$. The detailed simulation results and analysis can be found in [17].

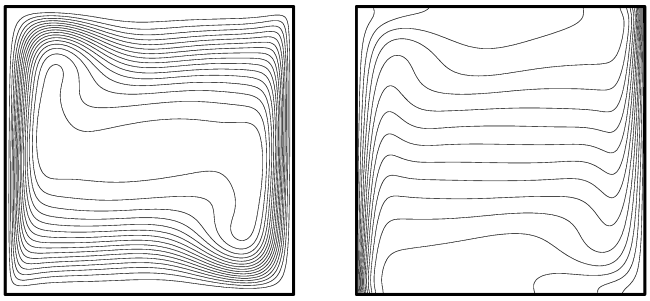

Figure 15 *Streamlines and isotherms for Ra = 10^6*

4.2 Natural convection in a concentric annulus between an outer square cylinder and an inner circular cylinder

In order to test the use of the TLLBM technique for the thermal problems with curved boundaries, numerical simulations of the natural convection in a concentric annulus between an outer square cylinder and an inner circular cylinder are carried out. Heat is uniformly generated within the inner circular cylinder, which is placed concentrically within the cold square cylinder.

The streamlines and isotherms for $Ra = 10^6$ and $rr = 5.0$, 2.5, 1.67 are shown in Figures 16 and 17, where rr is the aspect ratio. The detailed comparisons are shown in [18].

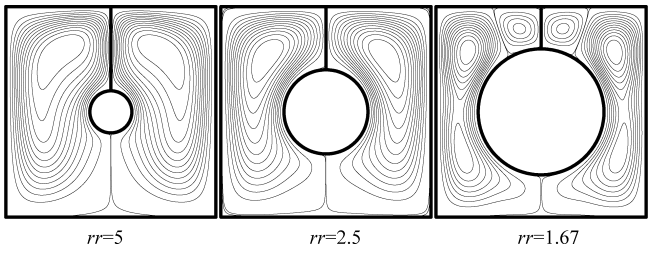

Figure 16 *Streamlines for Ra = 10^6*

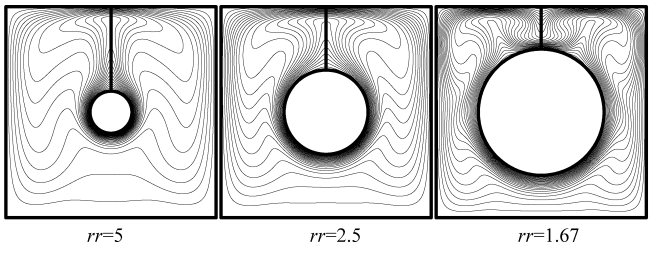

Figure 17 *Isotherms for Ra = 10^6*

4.3 The three-dimensional natural convection of air in a cubical enclosure

The current IEDDF thermal model has been extended to the three-dimensional case. The detailed description on this work can be found in [19]. We will only show some results here.

The streamlines and isotherms on the symmetric plane of $y = 0.5$ for $Ra = 10^5$ are shown in Figure 18. Figure 19 shows the profile of the mean Nusselt number along the y-direction on the heated wall of $x = 0$ for $Ra = 10^3$.

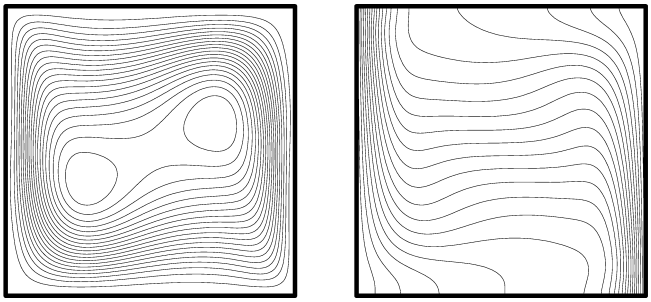

Figure 18 *Streamlines and isotherms at Ra = 10^5*

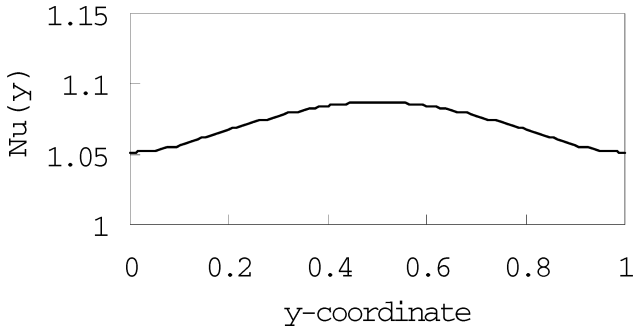

Figure 19 *Distribution of the mean Nusselt number in the y-direction for Ra = 10^3*

We would like to indicate that in above cases, all the TLLBM results are compared well with those from Navier-Stokes solvers, and the TLLBM computation only involves algebraic operations.

5 CONCLUSIONS

An explicit Taylor series expansion- and least square-based Lattice Boltzmann method has been successfully developed. Numerical simulations of the isothermal and thermal incompressible flows showed that the TLLBM is prospective in practical applications.

The beauty of the TLLBM is that it still keeps the local and explicit features of the standard Lattice Boltzmann method. Therefore, it is able to exploit fully the power of parallel computing. The other advantage of the present method is that it is easy for application to flow problems with complex geometry. Furthermore, the computational efficiency of the present method is competitive as compared with that of the standard LBE and the conventional CFD solvers.

REFERENCES

1 Chen, S. and Doolen, G.D. (1998) 'Lattice Boltzmann method for fluid flows', *Annu. Rev. Fluid Mech.*, Vol. 30, pp.329–364.

2 Frisch, U., Hasslacher, B. and Pomeau, Y. (1986) 'Lattice-gas automata for the Navier-Stokes equations', *Phys. Rev. Lett.*, Vol. 56, pp.1505–1508.

3 Wolfram, S. (1986) 'Cellular automaton fluids. 1: basic theory', *J. Stat. Phys.*, Vol. 45, pp.471–526.

4 Koelman, J.M.V.A. (1991) 'A simple Lattice Boltzmann scheme for Navier-Stokes fluid flow', *Europhys. Lett.*, Vol. 15, pp.603–607.

5 Qian, Y.H., d'Humières, D. and Lallemand, P. (1992) 'Lattice BGK models Navier-Stokes equation', *Europhys. Lett.*, Vol. 17, pp.479–484.

6 Bhatnagar, P.L., Gross, E.P. and Krook, M. (1954) 'A model for collision processes in gases, I: small amplitude processes in charged and neutral one-dimensional system', *Phys. Rev.*, Vol. 94, pp.511–525.

7 Shu, C., Chew, Y.T. and Niu, X.D. (2001) 'Least square-based LBM: a meshless approach for simulation of flows with complex geometry', *Phys. Rev. E.,* Vol. 64, No. 045701, pp.1–4.

8 Shu, C., Niu, X.D. and Chew, Y.T. (2002) 'Taylor series expansion- and least square-based Lattice Boltzmann method: two-dimensional formulation and its applications', *Phys. Rev. E*., Vol. 65, No. 036708, pp.1–13.

9 Shampine, L.F. (1994) *Numerical Solution of Ordinary Differential Equations*, Chapman & Hall.

10 Buchanan, J.L. and Turner, P.R. (1992) *Numerical Methods and Analysis*, New York, McGraw-Hill.

11 Chew, Y.T., Shu, C. and Niu, X.D. (2002) 'Simulation of unsteady incompressible flows by using Taylor series expansion- and least square-based Lattice Boltzmann method', *Int. J. Mod. Phys. C*, Vol. 13, No. 6, pp.719–738.

12 Niu, X.D., Shu, C. and Chew, Y.T. (2002) 'Numerical simulation of three-dimensional lid-driven cavity flow by Taylor series expansion and least squares-based Lattice Boltzmann method', *Int. J. Mod. Phys. C.*, Vol. 14, No. 7, pp.1–20.

13 Niu, X.D., Chew, Y.T. and Shu, C. (2003) 'An axisymmetric Lattice Boltzmann model for simulation of Taylor-Couette flow between two concentric cylinders', *Int. J. Mod. Phys. C.,* vol. 14, No. 6, pp.785–796.

14 Niu, X.D., Chew, Y.T. and Shu, C. (2003) 'Simulation of flows around an impulsively started circular cylinder by Taylor series expansion- and least squares-based Lattice Boltzmann method', *J. Comp. Phys*., Vol. 188, No. 1, pp.176–193.

15 Niu, X.D., Shu, C. and Chew, Y.T. (2003) 'Simulation of thermal flows by Taylor series expansion- and least square- based Lattice Boltzmann method coupling with macroscopic thermal equation', *Int. J. Mod. Phys. B*, Vol. 17, Nos. 1–2, pp.161–164.

16 Lim, C.Y., Shu, C., Niu, X.D. and Chew, Y.T. (2002) 'Application of Lattice Boltzmann method to simulate microchannel flows', *Phys. Fluids*, Vol. 14, No. 7, pp.2299–2308.

17 Shu, C., Peng, Y. and Chew, Y.T. (2002) 'Simulation of natural convection in a square cavity by Taylor series expansion- and least squares- based Lattice Boltzmann method', *Int. J. Mod. Phy. C.,* Vol. 13, No. 10, pp.1399–1414.

18 Peng, Y., Chew, Y.T. and Shu, C. (2003) 'Numerical simulation of natural convection in a concentric annulus between a square outer cylinder and a circular inner cylinder using the Taylor-series-expansion and least-squares-based Lattice Boltzmann method', *Phys. Rev. E*., Vol. 67, No. 026701, pp.1–6.

19 Peng, Y., Shu, C. and Chew, Y.T. (2003) 'A 3D incompressible thermal Lattice Boltzmann model and its application to simulate natural convection in a cubic cavity', *J. Comp. Phys.*, Vol. 193, pp.260–274.

20 Ghia, U., Ghia, K.N. and Shin, C.T. (1982) 'High-Re solutions for incompressible flow using the Navier-Stokes equations and a multigrid method', *J. Comp. Phys*., Vol. 48, pp.387–411.

21 Fuchs, L. and Tillmark, N. (1985) 'Numerical and experimental study of driven flow in a polar cavity', *Int. J. Numerical Methods Fluids*, Vol. 5, pp.311–329.

22 Ku, H.C., Hirsh, R.S. and Taylor, T.D. (1987) 'A pseudospectral method for solution of the three-dimensional incompressible Navier-Stokes equations', *J. Comp. Phys.*, Vol. 70, pp.439–462.

23 Coutanceau, M. and Bouard, R. (1977) 'Experimental determination of the main features of the viscous flow in the wake of a circular cylinder in uniform translation. Part 2: Unsteady flow', *J. Fluid Mech.*, Vol. 79, pp.257–272.

24 Bouard, R. and Coutanceau, M. (1980) 'The early stage of development of the wake behind an impulsively started cylinder for $40 < Re < 10^4$', *J. Fluid Mech.,* Vol. 101, pp.583–607.

25 Loc, T.P. and Bouard, R. (1985) 'Numerical solution of the early stage of the unsteady viscous flow around a circular cylinder: a comparison with experimental visualization and measurements', *J. Fluid Mech.*, Vol. 160, pp.93–117.

26 Chang, C.C. and Chern, R.L. (1991) 'A numerical study of flow around an impulsively started circular cylinder by a deterministic vortex method', *J. Fluid Mech.*, Vol. 233, pp.243–263.

27 He, X., Chen, S. and Doolen, G.D. (1998) 'A novel thermal model for the Lattice Boltzmann method in incompressible limit', *J. Comp. Phys.*, Vol. 146, pp.282–300.